actuators

MDPI

Article

Numerical Modeling and Structure Optimization for Magnetic Levitation Planar Machine Using PCB Coils

Han Zhang [1], Jiawen He [1], Xianze Xu [1], Rui Wang [2], Manman Xu [3,*] and Fengqiu Xu [1,*]

[1] School of Electronic Information, Wuhan University, Wuhan 430072, China; okzh611@whu.edu.cn (H.Z.); jv_hhh@whu.edu.cn (J.H.); xxz@whu.edu.cn (X.X.)
[2] Wuhan Yawei Electronics Co., Ltd., Wuhan 430072, China
[3] School of Mechanical Automation, Wuhan University of Science and Technology, Wuhan 430072, China
* Correspondence: xumanman@wust.edu.cn (M.X.); hncxu@whu.edu.cn (F.X.)

Abstract: Magnetically levitated (ML) systems that incorporate PCB coils represent a growing trend in precision machining, valued for their controllable current flow and high fill factor. The size of modern power devices is decreasing to enhance power density, minimize parasitic inductance, and reduce power losses. However, due to the high resistance of PCB coils, managing heat generation has become a significant area of study. This paper seeks to optimize PCB coil design to minimize power loss and control peak temperatures in ML systems, using a numerical model. An improved magnetic node model is employed to construct the magnetic fields of an ML system. The proposed optimization method considers the interdependencies among parameters to reduce overall power loss from coil resistance and switching losses in the H-bridge circuit, while enhancing heat dissipation efficiency in steady-state operation. A heuristic multi-objective optimization algorithm is employed to optimize the design of the ML actuator. The optimization process initially focuses on the PCB coils, with the magnet size held constant. Once the optimal coil parameters are identified, the magnet volume is optimized. By integrating a theoretical analysis with simulation, this approach effectively addresses the optimization challenges and achieves the desired performance for the ML actuator. Coils and magnets are constructed based on the optimized design and tested by the magnetic field simulation software Radia, confirming the feasibility of the approach. The method was also applied to a different type of ML system for comparison, demonstrating the universality of the proposed strategy. In this optimization effort, the maximum temperature reduction reached an impressive 50 °C.

Keywords: magnetic levitation; magnetic node model; PCB coils; power loss; optimal design

Academic Editors: Zigang Deng and Guang-Zhong Cao

Received: 30 November 2024
Revised: 8 January 2025
Accepted: 14 January 2025
Published: 16 January 2025

Citation: Zhang, H.; He, J.; Xu, X.; Wang, R.; Xu, M.; Xu, F. Numerical Modeling and Structure Optimization for Magnetic Levitation Planar Machine Using PCB Coils. *Actuators* **2025**, *14*, 33. https://doi.org/10.3390/act14010033

1. Introduction

Magnetically levitated (ML) technology offers a promising solution for applications in precision manufacturing, micro-manipulation, and the manufacture of semiconductors [1–3]. Since ML systems can move with six degrees of freedom (DoFs) without friction [4] and pollution [5], many researchers utilize ML technology to achieve precise motion and force control in various devices.

ML motion systems typically employ two types of coils as stators or actuators: traditional copper coils and PCB coils. A lot of studies are based on traditional coils [6–10]. While copper coils have long been used for their reliability, they occupy a large amount of space. To address this limitation, PCB coils have been introduced. Nowadays, PCB coils are widely utilized in modern technology due to their compact size, which conserves space, and

their higher filling factor, which enhances both levitation and propulsion performance. The generated magnetic force from these coils can support the mover, enabling linear motion by controlling the current through the coils. Significant research has been conducted on ML systems using PCB coils. For example, Kurita et al. developed a compact ML motor with flexible PCB to improve the filling factor through an optimized winding method [11]. Lu et al. designed a PCB stator with a one-dimensional (1D) Halbach array mover to create a novel long-stroke ML planar motor that achieves a higher filling factor and linear current increase with motion range [12]. NASA has also supported a project to develop a novel non-contact lunar railway utilizing a PCB coil track for operation on the moon [13]. Zou et al. presented a new ML planar motor system with 2D Halbach array based on PCB coils which needs less space [14].

To enhance the performance of ML systems, extensive research has been conducted over the years to optimize traditional copper coils and permanent magnets. Lee et al. proposed an optimization approach for both permanent magnets and copper coils by adjusting parameters such as magnet thickness, magnetization patterns, pole pitch, air gap length, and coil turns [15]. Saaideh et al. introduced a multi-objective optimization design to achieve maximum magnetic output while minimizing the mass, time constant, and stiffness of the actuator [16]. Li et al. focused on optimizing the width and length of permanent magnets and the air gap thickness to maximize magnetic flux density [17]. Guo et al. designed a system to achieve maximum magnetic output within the constraints of cost and space [18].

Despite recent advancements, research on optimizing ML systems with PCB coils to enhance overall performance remains limited. Existing optimization methods rarely address the heating challenges posed by the high resistance of PCB coils. As modern power devices shrink to improve power density, reduce parasitic inductance, and minimize power losses, thermal management has become a critical barrier to achieving higher power densities. Effective heat dissipation from the compact device to its surroundings is essential; insufficient thermal control can lead to elevated junction and board temperatures, ultimately jeopardizing the reliability of the PCB coil.

With effective thermal management increasingly challenging in electronics development due to the trend toward smaller device sizes [19–21], this optimization study addresses two key issues in planar PCB magnetic components: power loss and temperature regulation. Reducing the loss of heat is essential for maintaining optimal efficiency, while controlling the maximum device temperature is crucial for ensuring proper functionality and improving reliability [22,23].

In this study, three mathematical techniques—magnetic nodes, Gaussian quadrature, and coordinate transformation—are employed to construct an electromagnetic model. The magnetic node model is modified to accurately and simply describe the magnetic field around a permanent magnet [24], while coordinate transformation is used to build the model framework. Gaussian quadrature is applied to simplify the computational process [25], allowing for efficient calculation of the magnetic force. To minimize power loss caused by the resistance of PCB coils and the voltage drop and regulate the maximum temperature while operating, a heuristic multi-objective optimization algorithm, particle swarm optimization (PSO), is utilized to optimize the number of turns and thickness of the PCB coils. Based on the simulation results, the model was developed using Radia [26], and the outcomes calculated through magnetic nodes were compared with those from Radia to evaluate the feasibility of the design. The same optimization method was applied to other ML systems with different structures for comparison, further validating the reliability of the proposed design approach.

The rest of the paper is organized as follows. Section 2 introduces the construction of the optimization model, illustrating the process of the mentioned mathematical techniques. Section 3 illustrates how to build the objective function and optimize the PCB coils, while Section 4 demonstrates the experiment results. Section 5 concludes this article.

2. Numerical Model Design and Computation

2.1. Working Principle of ML System

Figure 1 comprises one unit of movers and stators. The mover consists of a magnet array, while the stator is made up of multiple layers of PCB coils. An adjustable air gap separates the mover from the stator, which can be controlled by varying the current through the coils. The current is assumed to be constant due to the extended region of coils beneath each magnet array.

Figure 2 presents two coordinate systems: {m} for the magnet array and {c} for the PCB coils. The {m} coordinate system is aligned parallel to the {c} coordinate system in space, with their origins ${}^{m}O$ and ${}^{c}O$ positioned along a common straight line. The force exerted on the mover of the ML system is equal in magnitude but opposite in direction to the force on the stator coil. This force can be determined using the Lorentz force equation.

The planar actuator can only be controlled stably in 6 DOFs since it has an active magnetic bearing. To achieve the stabilization, feedback control is essential in the magnetic levitation system. Controlling the mover requires at least six independently energized coils. Given that the total force and torque are calculated by summing the contributions of each individual PCB coil when the mover is modeled as a rigid body, the models in this paper are developed for a single coil. The synthesis and optimization of configurations with multiple coils are beyond the scope of this study.

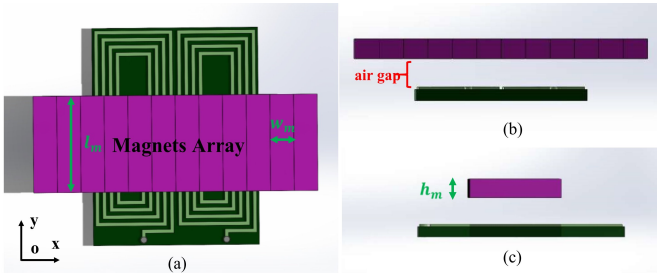

Figure 1. One unit of the proposed ML system utilizing PCB coils in (**a**) top, (**b**) front, and (**c**) side views.

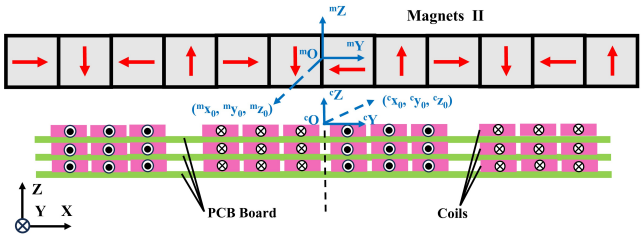

Figure 2. The cross-section of Magnets II and its corresponding active coils.

2.2. Construction of Numerical Model

Developing an accurate magnetic model is a prerequisite for structural optimization research. A precise magnetic model ensures the effectiveness of the optimization process, enables more accurate magnetic control in the ML system, and provides realistic force feedback. The construction of the numerical model involves developing both the magnetic field model and the force model. The magnetic field model is created using the magnetic

nodes, which provides the magnetic flux density of the system. The magnetic force is then calculated using the Lorentz integral formula, based on the derived expression for magnetic flux density.

2.2.1. Magnetic Nodes

This method treats the magnetic field produced by a permanent magnet as a superposition of magnetic fields from several independent nodes, known as 'magnetic nodes' [24]. Figure 3a illustrates the distribution of 8 magnetic nodes within a cuboid magnet. Therefore, the magnetic flux density generated by the permanent magnet at point ${}^{m}A$ is equivalent to the vector sum of the magnetic flux densities produced by the excitation of these 8 magnetic charges:

$$ {}^{m}B({}^{m}A) = \sum_{i=1}^{K} {}^{m}B_i({}^{m}N_i, {}^{m}A) \tag{1} $$

where i is the number of magnets, K is 8 in the rectangular magnets, and ${}^{m}N_i$ represents the equivalent magnetic node located at each vertex of the permanent magnet. The detailed derivation of ${}^{m}B({}^{m}A)$ can be found in [19].

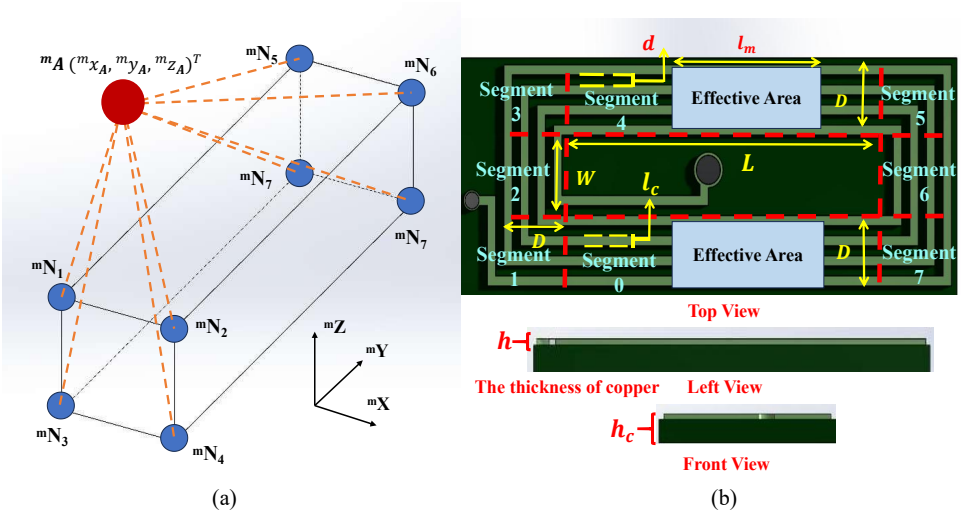

Figure 3. Diagram of (**a**) magnetic nodes and (**b**) the top view of segments in a typical coil.

2.2.2. Coordinate Transformation

During the operation of the magnetic suspension system, the permanent magnet, acting as a moving element, will exhibit relative motion with respect to the stator coil. Magnetic vectors from different coordinate systems cannot be directly used for calculating the magnetic force. To accurately construct the magnetic force model of the system, the magnetic force should be calculated within the coordinate system aligned with the stator, allowing for a more precise determination of the magnetic force. The transformation matrix that converts the coordinates of the magnet system to the coil's coordinate system is denoted as ${}^{c}R_m$, while the translation vector in the coil's coordinate system is represented as ${}^{c}P_m$. Consequently, the magnetic flux density in the stator coordinate system is given by

$$ \begin{aligned} {}^{c}B({}^{c}A) = \sum_{i=1}^{K} {}^{c}R_m \cdot {}^{m}B_i({}^{c}R_m \cdot {}^{m}N_i + {}^{c}P_m, \\ {}^{c}R_m \cdot {}^{m}A + {}^{c}P_m) + {}^{c}P_m \end{aligned} \tag{2} $$

2.2.3. Computation of Magnetic Force

The magnetic force generated by the permanent magnet and the magnetic force produced by the coil are a pair of equal and opposite interaction forces. Therefore, once the analytical solution for the magnetic flux density of the ML system is obtained, the Lorentz force integral formula [27] can be employed to determine the magnetic force of the permanent magnet:

$$^{c}\mathbf{F} = \iiint_{V_c} {}^{c}\mathbf{J} \times {}^{c}\mathbf{B} dV_c \tag{3}$$

where $^{c}\mathbf{B}$ is the magnetic flux produced by permanent magnets, the whole dV_c is equal to $d^c x d^c y d^c z$ of the coil, and $^{c}\mathbf{J}$ is the vector of current density of the PCB coils. The vector of $^{c}\mathbf{J}$ is $[I_c N_c / D h_c, 0, 0]^T$, N_c is the total number of coils, h is the thickness of the PCB coils, I_c is the current flow in a single wire, and D is the distance from the inner coil to the outer coil for each side, shown in Figure 3. D can be calculated as

$$D = N l_c + (N-1)d \tag{4}$$

where N is the number of turns of the PCB coil per layer, d is the gap between each wire, and l_c is the width of a single coil. According to the Lorentz principle, the magnetic force is determined by identifying the primary current-carrying regions of the coil. Figure 3b depicts the segmentation of a typical PCB coil. Since the magnetic field in the air gap below the 1D Halbach permanent magnet array diminishes to zero outside the array region [28], the current-carrying sections are confined to the long sides of the PCB coils. Therefore, the primary sources of magnetic force excitation in the moving unit are parts of segments 0 and 4 (the part under the magnets) for each coil, as shown in Figure 3b. The relationship between the mover and stator can be described through a relative translating vector $P = [p_x, p_y, p_z]^T$. To simplify the optimization process, the translating vector in this study is set to $[0, 0, 0]^T$. According to Equation (3), the magnetic force acting on the magnetic array illustrated in Figure 1a should be

$$^{c}\mathbf{F} = \int_{-h}^{0} \left(\int_{0}^{D} - \int_{D+W}^{2D+W} \right) \int_{p_x - \frac{l_m}{2}}^{p_x + \frac{l_m}{2}} {}^{c}\mathbf{J} \times {}^{c}\mathbf{B} dV_c \tag{5}$$

where l_m is the length of a magnet.

2.2.4. Gaussian Quadrature

Gaussian quadrature divides the integral function into multiple nodes and calculates the value at each node. These values are then weighted and summed to approximate the result of integral [29]. Following the error estimation method outlined in [28], this work applies the eighth-order rule, specified as follows:

$$\int_{x_2}^{x_1} f(x)dx = \frac{x_2 - x_1}{2} \sum_{g=0}^{7} w_g f\left(\frac{x_2 + x_1}{2} + \lambda_g \frac{x_2 - x_1}{2} \right) \tag{6}$$

where λ_g and w_g are the nodes and weights of the Gaussian quadrature. As illustrated in Figure 3b, only two segments (segments 0 and 4) are effective. Therefore, the formula for calculating the magnetic force in the ML system, after applying Gauss numerical integration and simplifying with Equation (4), is given as follows:

$$^{c}\mathbf{F} = -\frac{h l_m D}{8} \sum_{n_1}^{8} \sum_{n_2}^{8} \sum_{n_3}^{8} {}^{c}\mathbf{J} \times {}^{c}\mathbf{B} \left({}^{c}\mathbf{G_0} - {}^{c}\mathbf{G_4} \right) \tag{7}$$

$$^{c}\mathbf{G_0} = (\frac{D}{2}\lambda_g + \frac{l_m}{2} + \frac{D}{2}, \frac{W}{2}\lambda_g, \frac{h}{2}\lambda_g) \tag{8}$$

$$^{c}\mathbf{G_4} = (\frac{D}{2}\lambda_g - \frac{l_m}{2} - \frac{D}{2}, \frac{W}{2}\lambda_g, \frac{h}{2}\lambda_g) \tag{9}$$

where $^{c}\mathbf{G_0}$ and $^{c}\mathbf{G_4}$ represent the Gaussian quadrature nodes for segments 0 and 4, respectively. The symbols W and l_m denote the inner width and the effective length of the PCB coils located directly beneath the magnets, with l_m also being equivalent to the magnet length. In this study, the vector $^{c}F = [^{c}f_x, ^{c}f_y, ^{c}f_z]^T$ represents the forces per unit of current along the x, y, and z axes.

2.3. Heat Transfer Equation for PCB

For high-power applications, effective heat dissipation is crucial for ensuring long-term reliability, and potential temperature fluctuations must be accounted for during the design phase rather than only during verification [30]. As the temperature rises, the resistance of the coil generally increases due to the positive temperature coefficient of copper and other conductive materials. This behavior can be described by the equation

$$R_t = R_0(1 + \alpha\Delta T) \tag{10}$$

where R_t is the resistance at temperature T, R_0 is the resistance at the reference temperature, α is the temperature coefficient of resistance, and ΔT is the change in temperature. The increase in resistance results in higher power losses, which in turn can further amplify heating.

However, this study focuses on the thermal conditions at equilibrium, and subsequent optimization is based on balanced thermal equations. At equilibrium, heat transfer within the winding of magnetic components is predominantly governed by conduction. Under steady-state conditions, the thermal resistance of a PCB coil can be expressed in the following form:

$$R_c = \frac{L}{kA} \tag{11}$$

where k is the thermal conductivity of the material, L the length of the path, and A is the the cross-sectional surface of the considered path.

In thermal networks, the resistance to heat flow is represented by thermal impedance, which is composed of resistive and capacitive elements. These resistances describe how the component behaves when it reaches steady-state conditions. The behavior of the component is determined by the resistances during steady-state conditions, while thermal inertia is represented by the capacitances [31]. Magnetic components, known for their high thermal inertia, respond to changes in applied power like an overdamped system [32]. As a result, the most significant condition during stable operation occurs at steady state, where the maximum temperature is reached. The model focuses on steady-state analysis, considering only the real part of the thermal impedance.

In magnetic components, when a fluid is present, convection occurs. The temperature of the PCB coil is influenced by the fluid's properties, the convective surface area, as well as the speed and temperature of the fluid flow [32]. The steady-state temperature can be determined using the following equation:

$$T = T_0 + \frac{Q_c}{\alpha A} \tag{12}$$

where α represents the heat transfer coefficient (HTC), Q_c is the heat generated by the PCB coil, A is the sum of a PCB surface area, T_0 is the room temperature, and T is the operating temperature at steady state. The value of α is influenced by the properties of the fluid near the cooled surface, which change depending on the temperature. To estimate

the heat transfer coefficient for each surface of the object, experimental correlations based on different surface geometries and orientations can be applied, with fluid properties evaluated at the film temperature [33]. The analytical solution for temperature, using a Fourier series approach, was primarily derived based on the assumed average heat transfer coefficient (HTC) of the PCB surface [34]. In this study, the HTC was selected to be 13 W/m^2K [35].

2.4. Power Loss Caused by Resistance and Voltage Drop

The other significant issue negatively impacting the performance of the ML system is the power loss resulting from the coil resistance and the switching circuit. This issue warrants careful attention because the resistance of the coil directly influences the coil size design, while the voltage drop caused by the H-bridge circuit complicates the selection of an appropriate device for operating the system. In an H-bridge circuit, switching components (such as MOSFETs or IGBTs) operate at high frequencies. By varying the duty cycle, or the ratio of "on" time to "off" time in each switching cycle, the voltage applied across the motor terminals can be precisely controlled. This voltage regulation primarily affects the current and magnetic field strength within the planar, enabling accurate control of its motion and ensuring overall system stability. Power losses are caused by an internal resistance or voltage drop across the switching components when they are in the conducting state. The total energy loss, which stems from both the PCB coil resistance and the drive voltage, is calculated as follows:

$$Q = Q_c + Q_v = I_c^2 R_c + V I_c \tag{13}$$

where Q_c and Q_v are the power losses of the coils and driven voltage, R_c is the coil resistance, and V is the voltage drop across the switch (H-bridge). R_c and I_c can be calculated as

$$R_c(N) = \frac{(2\rho_c N_c(W+L) + 4N_c(N_c-1)(l_c+d))P}{kh_c l_c} \tag{14}$$

$$I_c(h_c, N_c) = \frac{G_{mass}}{{}^c f_z(h_c, N_c)} \tag{15}$$

where ρ_c denotes the resistivity of the material, l_c represents the width of a single wire, P is the number of layers, d is the gap between adjacent wires, and G_{mass} is the weight of the load.

3. Optimal Design for the ML System

To achieve efficient performance while minimizing structural costs, many designs undergo optimization [33–35]. In this paper, a typical ML system with a 1D Halbeck array is taken as an example; the system structure is demonstrated in Figure 4. The key parameters considered in the magnetic suspension system analyzed in this paper include the total coil height (h_c) (Figure 3b), and the number of coil turns in a single layer (N_c) of the PCB. Since the h_c contains the thickness of the prepreg layer (h_p), core (h_{core}), and solid mask (h_s), the relationship among these parameters can be illustrated as

$$h_c = h \times N_c + h_p \times (N_c - 1) + h_{core} + 2h_s \tag{16}$$

where h, h_p, h_{core}, and h_s are constant. Performance criteria include the magnetic force of the output along the z-axis, the power consumption of the system, and the operating temperature of the device. In this study, a heuristic optimization algorithm is used to determine the design parameters, ensuring the best possible optimization results. In the initial optimization step, the size of the PCB coil is optimized. In the subsequent step, the coil parameters are kept constant while the magnet thickness is optimized.

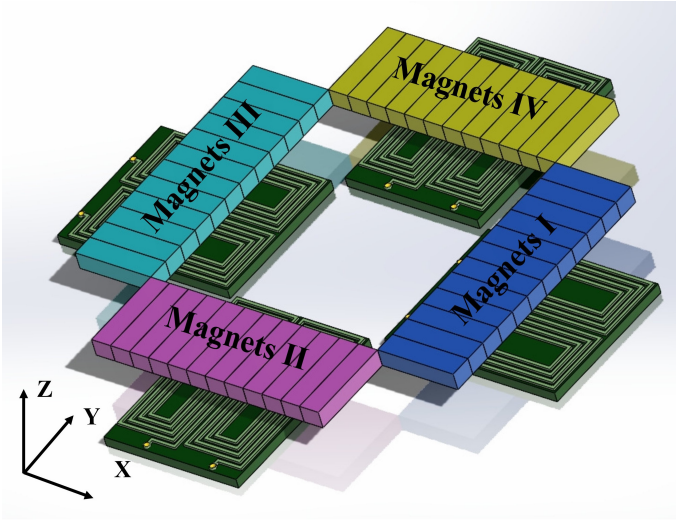

Figure 4. A typical example of an ML system with 1D Halbach array.

3.1. Optimization of Variables and Objective Functions

In this study, three parameters of the ML system, $Opt = (h_c, N_c, h_m)$, are optimized. The initial focus of optimization is the coil, with the goal of determining its optimal parameters, defined as $Opt_c = (h_m, N_c)$. Variations in the coil dimensions significantly impact current density and resistance, which in turn affect the power output and energy consumption of the ML system. The coil parameters, Opt_c, are optimized to minimize power consumption while improving heat dissipation.

By multiplying the power consumption Q with the maximum stable system temperature T, this work captures the combined effect of both factors. This product effectively amplifies the impact when both power consumption and temperature are elevated, ensuring the optimization process gives greater emphasis to performance issues in extreme cases, such as when both temperature and power consumption are excessively high. The reason for not considering the sum of these physical quantities is due to the significant difference in scale—power consumption typically has much larger values than temperature. Consequently, adding them would diminish the influence of temperature on the objective function, resulting in suboptimal performance during the optimization. Therefore, the objective function is formulated as

$$f_{obj} = QT = \frac{Q_c Q}{\alpha A} + T_0 Q \tag{17}$$

The relative importance of temperature and power consumption can be adjusted according to the judgment of the designer or based on specific system requirements. The designer can assign weights or use normalization techniques to adjust the influence of each parameter to reflect their practical significance. In this design, the focus of the work is on optimizing Equation (17).

This objective function aims to minimize heat loss in the system while keeping the operating temperature within acceptable limits. The optimization process focuses on adjusting the coil thickness to adjust the PCB cooling surface and modifying the coil turns to optimize its resistance. These adjustments help achieve the objectives of this optimization study. The second optimization target is the thickness of the magnets, defined by the variable $Opt_m = (h_m)$. After obtaining the optimized coil parameters, the coil dimensions are fixed, and h_m becomes the variable in a subsequent optimization, using the same objective function.

3.2. Optimization Algorithms and Constraints

Particle swarm optimization (PSO) is an advanced heuristic algorithm well suited to solve multimodal and single-modal problems due to its simple structure, high optimization efficiency, and robust global convergence [36]. It has been widely applied to optimization problems in various fields [37–42]. From the previous section, the first constraint optimization problem is described as

$$\begin{aligned} &\min \quad f_{obj}(h_c, N_c, h_m) \\ &s.t. \quad \begin{cases} h_c > 0 \\ N_c > 0 \\ l_c = \frac{R-(N-1)d}{N} > 0 \\ h_m = 8 \end{cases} . \end{aligned} \tag{18}$$

The thickness of the magnets is fixed at 8 mm, while the two variables of the PCB coils, h_c and N_c, are optimized initially.

Following the initial optimization, the coil parameters are kept constant. The objective function is then applied to optimize the height of the magnets. The constraints for the second optimization are as follows:

$$\begin{aligned} &\min \quad f_{obj}(h_c, N_c, h_m) \\ &s.t. \quad \begin{cases} h_m > 0 \\ h_c = constant \\ N_c = constant \end{cases} . \end{aligned} \tag{19}$$

Figure 5 illustrates the PSO process used in this study. Initially, the magnet dimensions are set to a random value. The magnetic node model is then used to calculate the objective function f_{obj} for each particle, allowing for the determination of the optimal number of coil turns and coil thickness through the PSO algorithm. Once these optimal values are achieved, the dimensions of the PCB coil are fixed. Subsequently, the optimization process focuses on the magnet height, h_m, using the same objective function f_{obj} and applying the same optimization procedure. This two-step optimization method has not been applied to ML systems before. The approach helps manage system complexity by addressing the coil and magnet separately, given their distinct design variables and constraints. The structure allows this work to focus on the specific optimization goals for each component while maintaining their interdependence within a unified framework, ensuring overall system performance.

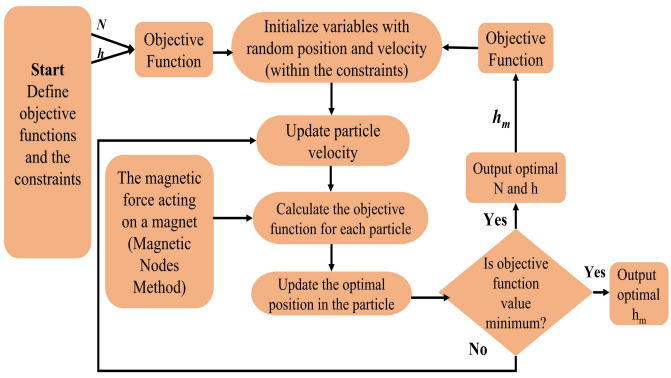

Figure 5. Flow chart of PSO in proposed method.

4. Validation and Verification of Magnetic Model and Optimization Process

To confirm the feasibility of the proposed magnetic model, three experimental configurations (A1, A2, and A3) were designed. These experiments aim to validate the accuracy of the model, reduce energy loss, lower the operating temperature of the ML system, and evaluate the robustness and general applicability of the optimization methodology.

A1: This experiment compares the magnetic model constructed in MATLAB with an equivalent model built in Radia. The objective is to assess the feasibility and accuracy of the modified magnetic node model, ensuring that it can reliably represent magnetic behaviors under varying configurations.

A2: In this phase, the proposed PSO optimization method is applied to an ML system with a 1D Halbach array. Key parameters of the PCB coil and magnets are adjusted within this setup to enhance the overall performance of the ML system, targeting reductions in energy loss and improved thermal management.

A3: The optimization method is further tested on an ML system with a 2D Halbach array, as illustrated in Figure 6, to verify its generality and correctness. This configuration examines the adaptability of the optimization approach across different magnetic arrangements, underscoring its versatility and effectiveness.

The initial fixed parameters for the ML system using a 1D Halbach array are detailed in Table 1. These constants provide a baseline for assessing improvements and validating the proposed impact of optimization on system performance.

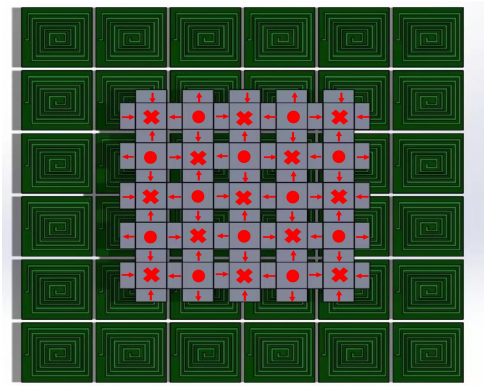

Figure 6. A typical example of ML system with 2D Halbach array.

4.1. Feasibility of the Modified Magnetic Node Model

To validate the feasibility of the modified magnetic node model, the results are compared with those obtained using Radia. The magnetic node modeling approach was implemented in MATLAB. Figure 7 illustrates the magnetic force per unit current distribution within the model, which was developed using magnetic nodes and Radia. The simulation incorporates a coil thickness of 8.32 mm with seven wire turns and displays the distribution of force per unit current across one magnetic period. The MATLAB and Radia results shown in Figure 7 demonstrate strong agreement.

Table 2 presents the magnetic force per unit current generated by PCB coils of varying sizes, comparing results from both the magnetic node method and Radia for the 1D configuration. The data clearly demonstrate that, across different current densities and coil thicknesses, the outcomes are closely aligned with those obtained from the Radia simulations. This consistency confirms the accuracy and reliability of the modified magnetic node method.

Table 1. Initial constant parameters of ML system.

Parameter	Value
Heat transfer coefficient (α)	15 W/m^{2}k
Inner length of the coil (L)	60 mm
Inner width of the coil (W)	10 mm
Distance from the inner to the outer coil (D)	10 mm
Thickness of copper (h)	0.2 mm
Distance between each wire (d)	0.1 mm
Resistivity (ρ_c)	1.72×10^{-5} Ω·mm
Air gap (g)	1.5 mm
Length of the magnet (l_m)	40 mm
Width of the magnet (w_m)	10 mm
Remanence (B_r)	1.2 T
The relative permeability of magnet (μ_r)	1.1
Density of the magnet (ρ_m)	7.5×10^{-3} g/mm^2
Height of the magnets (h_m)	8 mm
Constant weight of the stator (G_m)	20 N
Room temperature	25 °C

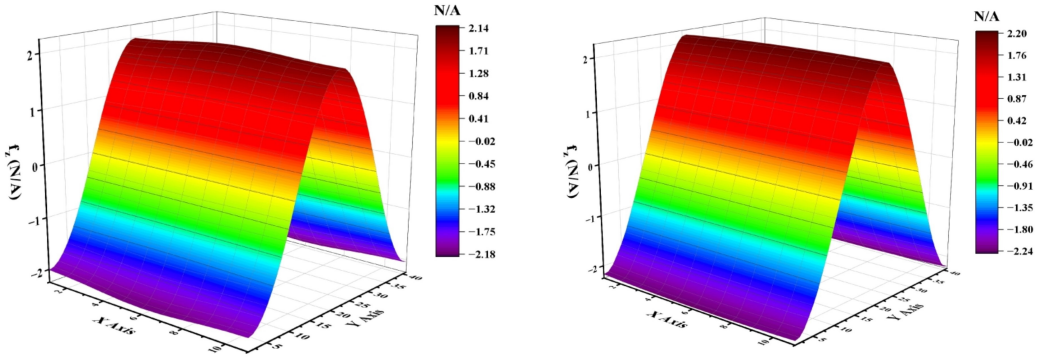

Figure 7. Magnetic force distribution of the ML system with 1D Halbach array using (**a**) magnetic nodes and (**b**) Radia.

Table 2. Comparison of magnetic force per unit current along the z-axis generated by PCB coils of different sizes: MATLAB vs. Radia.

Type	Size		Results	
	Turns (turns)	Thickness (mm)	f_z in MATLAB (N/A)	f_z in Radia (N/A)
Figure 4	3	3.84	0.599	0.605
	3	4.48	0.666	0.675
	3	5.76	0.782	0.796
	3	7.68	0.917	0.936
	7	8.32	1.905	1.950
	10	8.32	2.858	2.737
	13	8.32	3.810	3.647

4.2. Optimization Process and Results

In the PSO optimization process, a population size of 50 particles is utilized to ensure a sufficiently diverse search space, while the algorithm runs for 14 iterations to enable thorough exploration and convergence. The inertia weight is set at 0.5, maintaining a balance between global and local search capabilities. The cognitive coefficient (C_1) and social coefficient (C_2) are assigned values of 1.5 and 2.0, respectively, to fine-tune the balance

between individual exploration and group cooperation, facilitating effective exploitation of the search space.

The initial magnet height is randomly initialized at 8 mm to introduce variability in the starting conditions. Throughout the experiment, the voltage drop of the H-bridge circuit is varied within the range of 1 V to 10 V, which influences the resulting optimal PCB coil dimensions. The optimization process at a voltage drop of 4 V is illustrated in Figure 8, highlighting the step-by-step convergence towards an optimal design, which proves the validity and reliability of the optimization design. The optimal parameters for the PCB coil under a voltage drop of 4 V are clearly defined as three turns per layer and a thickness of 9.2 mm. It is also evident that during the optimization process, the increase in coil thickness leads to a reduction in system temperature. This is due to the greater thickness expanding the PCB surface, thereby improving heat dissipation efficiency.

Figure 9a,b present the optimized coil size. As the voltage drop across the switch rises, the number of turns in the PCB coil also grows. The thickness of the PCB coil remains constant at 9.2 mm. This is primarily due to the fact that a higher voltage drop leads to greater power loss. To mitigate this loss, the optimization process increases the number of turns, thereby enhancing the magnetic force generated per unit of current. This adjustment allows the current of the system to be reduced, thereby minimizing localized heating and power loss. Figure 9c displays the progression of the objective function values across iterations, showcasing the ability of the algorithm to gradually refine the design.

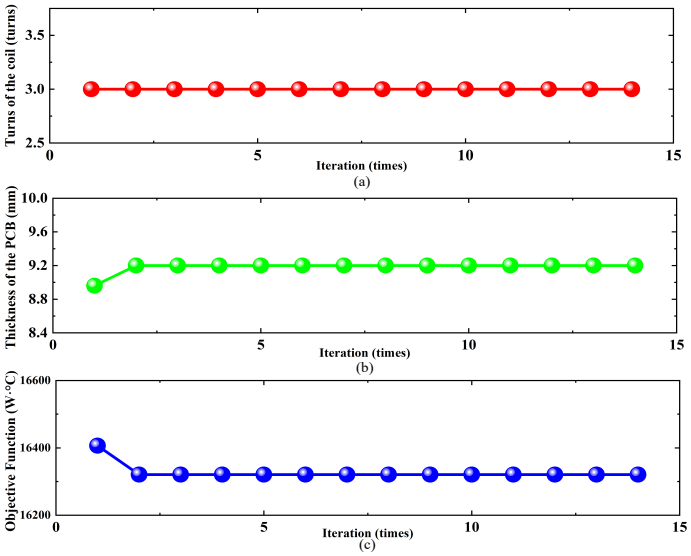

Figure 8. Iteration process for PCB coil optimization at a voltage drop of 4 V: (**a**) number of turns, (**b**) PCB coil thickness, and (**c**) objective function value.

In the subsequent phase, the PCB coil size was held constant, and the magnet height was optimized based on the same objective function. The height of the magnets in the 1D Halbach array was optimized from 8 mm to 12 mm during the second optimization phase. Increasing the magnet thickness enhances the magnetic force generated per unit of current, which reduces the current and consequently lowers power consumption and system temperature. However, once the magnet reaches a certain thickness, the magnetic field strength becomes saturated, and further increases in thickness do not lead to a significant improvement in the magnetic force per unit of current. Therefore, 12 mm was determined to be the optimal magnet thickness for this ML system.

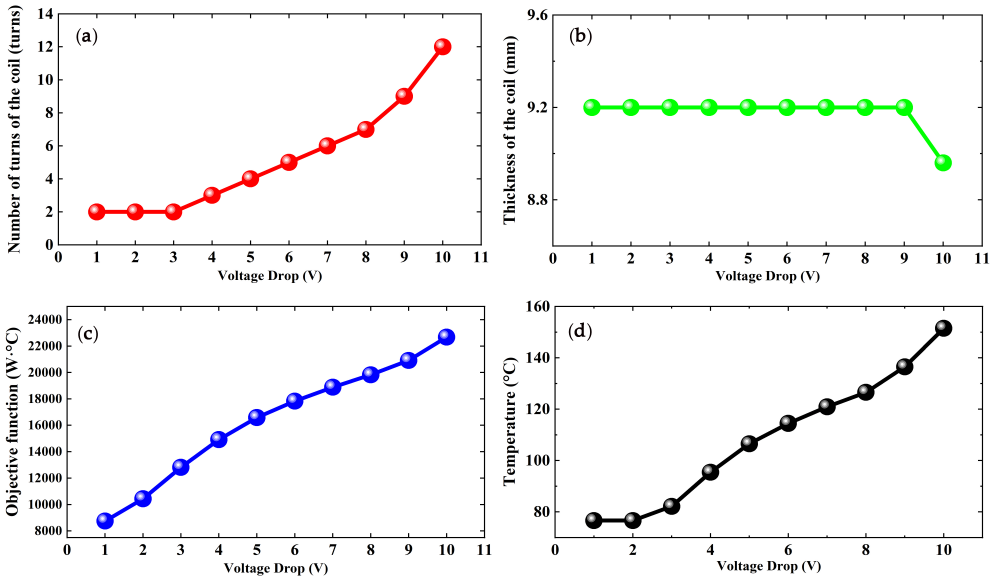

Figure 9. Optimized results: (**a**) number of turns, (**b**) coil thickness, (**c**) objective function, and (**d**) operating temperature values for 1D Halbach arrays.

The results for the objective function value are depicted in Figure 10. When comparing these results to the values in Figure 9c, it is evident that the objective function achieves significantly lower values after optimizing the magnet height. These visualizations emphasize the effectiveness of the optimization approach in meeting the targeted performance metrics for the PCB coil across different conditions. Notably, the operating temperature of the ML system in Figure 10b shows a significant reduction. For instance, at a voltage drop of 9 V, the temperature of the system decreases by 50 degrees. This is because the optimal thickness of the magnets reduces the current in the system, resulting in lower power consumption and a decrease in operating temperature.

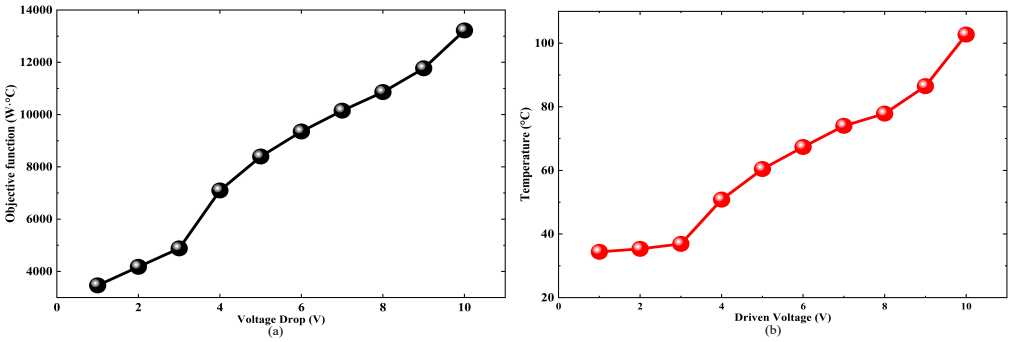

Figure 10. Optimal results for (**a**) the objective function values and (**b**) operating temperature of the second optimization for 1D Halbach arrays.

4.3. Effectiveness and Versatility of the Proposed Optimization

The same optimization process was applied to an ML system with 2D Halbach arrays, as illustrated in Figure 6, to confirm its feasibility and adaptability. The range of the drive voltage in this case remained consistent with that used in the previous 1D Halbach array experiment, ensuring comparability across configurations. Figure 11 illustrates the PSO iteration process for optimizing the PCB coil parameters at 4 V within the 2D Halbach array ML system. The optimal parameters under a voltage drop of 4 V are clearly defined as seven turns per layer and a thickness of 9.6 mm. As the thickness of the PCB coil increases, the temperature decreases due to the expanded heat-radiating surface of the

PCB. The iteration results demonstrate a well-defined convergence trend, underscoring the effectiveness of the optimization approach.

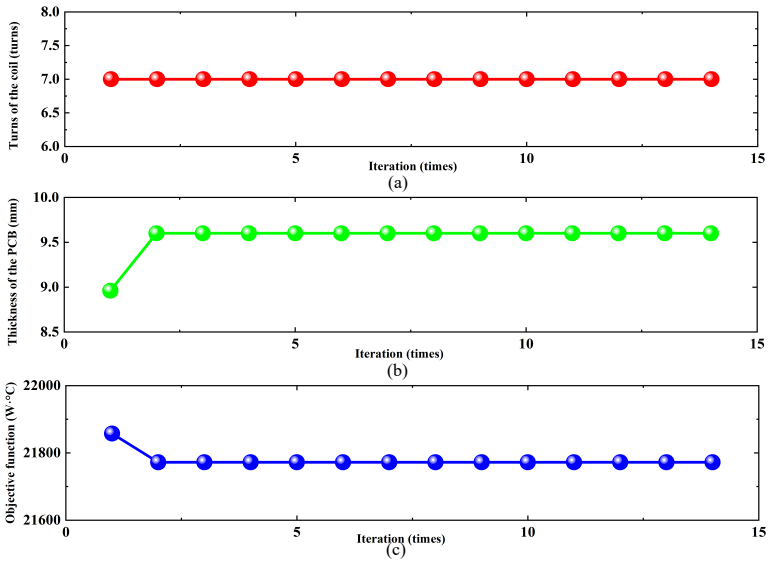

Figure 11. Iteration process of PCB coil optimization at a voltage drop of 4 V: (**a**) turns, (**b**) thickness of the PCB coil, and (**c**) the value of objective function for ML system with 2D Halbach array.

Following the initial optimization stage, Figure 12 presents the optimized results with fixed PCB coil parameters. As the voltage drop increases, the number of coil turns per layer rises from 1 to 14, while the PCB thickness remains constant at 9.6 mm. The higher voltage drop results in greater power loss, prompting an increase in coil turns to mitigate the loss. This adjustment enhances the force per unit current. The results in the PCB coil exhibits the same trend as the system with a 1D Halbach array, thereby confirming the accuracy of the method.

In this phase, the magnet thickness is refined, transitioning from an initial random value of 8 mm to an optimized value of 11 mm. The increased thickness improves the magnetic force per unit current and reduces the current of the system, thereby lowering power consumption. At 11 mm, the thickness generates a saturated magnetic field, and any further increase would not result in a significantly enhanced magnetic force. The values of the objective function from the second optimization are shown in Figure 13, where a reduction in the objective function value is observed compared to the first optimization. This improvement underscores the robustness and effectiveness of the proposed optimization methodology in enhancing system performance across multiple configurations.

Based on the previous optimization results, two types of ML systems were developed, as illustrated in Figure 14. For the ML system utilizing a 2D Halbach array, the stator weight is 10 N in the actual design, and the optimal parameters are determined accordingly. Similarly, the ML system with a 1D Halbach array was designed based on the previous optimization results, accommodating the same 23 N load. The detailed parameters are provided in Table 3. In future work, we aim to implement effective control strategies for these systems.

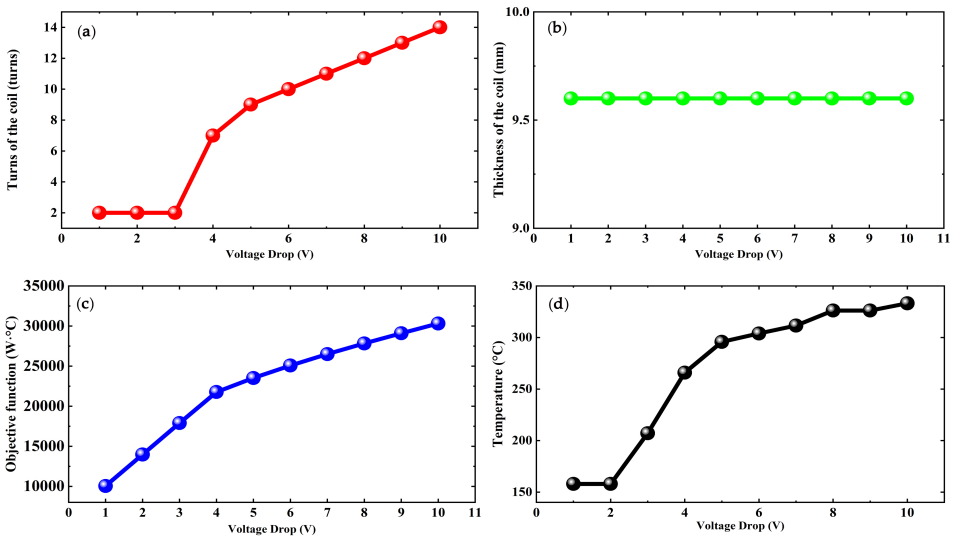

Figure 12. Optimized results: (**a**) number of turns, (**b**) coil thickness, (**c**) objective function values, and (**d**) operating temperature for 2D Halbach arrays.

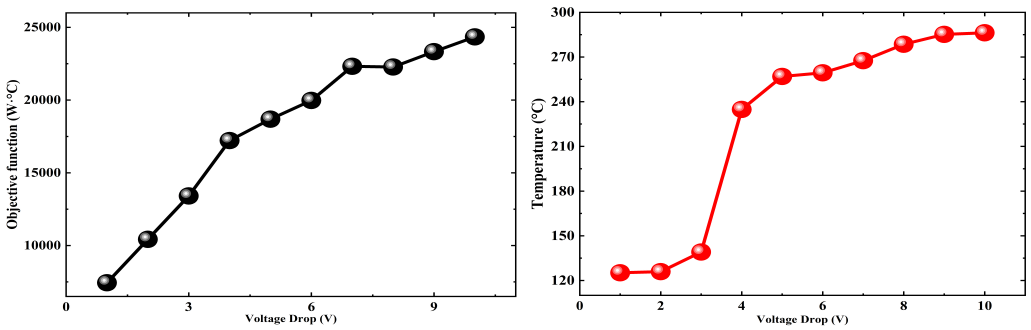

Figure 13. Optimal results for the objective function values of the second optimization for 2D Halbach arrays (with a load of 2.3 kg).

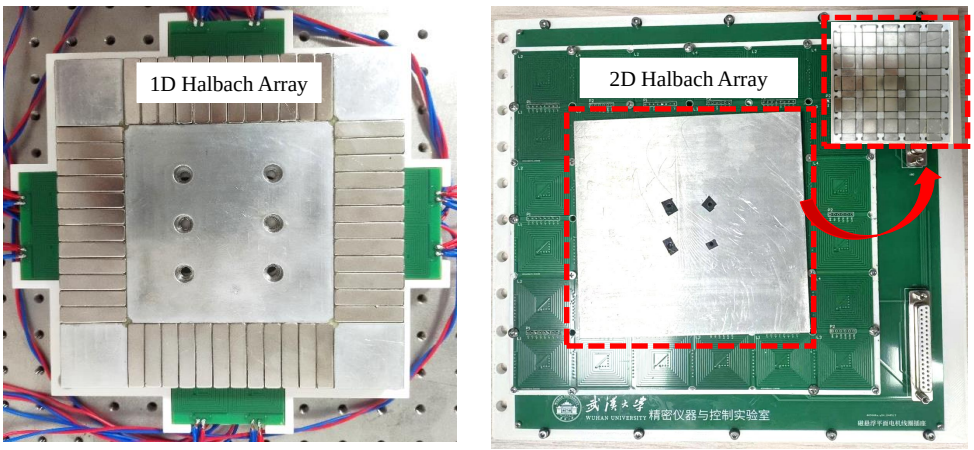

(a) (b)

Figure 14. Actual design of ML system with (**a**) 1D and (**b**) 2D Halbach arrays using PCB coils.

Table 3. Main structural parameters of ML planar with 1D and 2D Halbach arrays.

Basic Parameter	Values for 1D ML System	Values for 2D ML System
Length of the magnets (l_m)	40 mm	16 mm
Width of the magnets (w_m)	10 mm	8 mm
Height of the magnets (h_m)	12 mm	11 mm
Constant weight of the stator (G_m)	23 N	10 N
Thickness of the PCB coil (h_c)	9.2 mm	8.32 mm
Total width of one PCB coil (w_c)	30 mm	48 mm
Total length of one PCB coil (l_c)	80 mm	48 mm
Total turns of one PCB coil (N_c)	180 turns	171 turns
Number of layer of PCB	20 layers	19 layers
Thickness of the copper (h)	0.2 mm	0.2 mm

5. Conclusions

This paper introduces a numerical model for an ML system equipped with a PCB coil and a 1D Halbach array, utilizing a modified magnetic node method combined with Gaussian quadrature. The magnetic model is simulated in MATLAB and then optimized. A comparison of the simulation results from MATLAB and Radia verifies the accuracy and robustness of the proposed modified approach. Unlike conventional optimization approaches, this work emphasizes minimizing power loss caused by coil resistance, driving voltage, and the maximum operating temperature of the system, while ensuring system stability. The optimization process focuses on adjusting the PCB coil dimensions and magnet thickness, with PSO applied to efficiently navigate the search space, avoiding local optima and accelerating convergence. To demonstrate the versatility of the method, a 2D Halbach array is also optimized. The results confirm that this method enables efficient and precise optimization, providing valuable insights for the design and enhancement of ML systems utilizing PCB coils.

Author Contributions: Conceptualization, F.X.; methodology, H.Z. and J.H.; formal analysis, H.Z.; investigation, H.Z.; data curation, H.Z.; writing—original draft preparation, H.Z.; writing—review and editing, F.X.; supervision, F.X., X.X. and M.X.; funding acquisition, F.X., X.X. and R.W. All authors have read and agreed to the published version of the manuscript.

Funding: This research was funded by the National Key Research and Development Young Scientist Program (Grant No. 2022YFF0605400), and Hubei Province innovation plan project (Grant No. 2024DJC046, 2024KJB332 and 2023BAB050).

Data Availability Statement: The raw data supporting the conclusions of this article will be made available by the authors on request.

Conflicts of Interest: Author Rui Wang was employed by the company Wuhan Yawei Electronics Co., Ltd. The remaining authors declare that the research was conducted in the absence of any commercial or financial relationships that could be construed as a potential conflict of interest.

References

1. Pieters, R.; Tung, H.; Charreyron, S.; Sargent, D.F.; Nelson, B.J. RodBot: A rolling microrobot for micromanipulation. In Proceedings of the 2015 IEEE International Conference on Robotics and Automation, Seattle, WA, USA, 26–30 May 2015; pp. 4042–4047.
2. Jeong, J.; Ryu, J.; Gweon, D. Feedforward reference compensation using bilinear interpolation for long range motion of six degrees-of-freedom magnetic levitation planar motor. In Proceedings of the 2017 8th International Conference on Mechanical and Aerospace Engineering, Prague, Czech Republic, 22–25 July 2017; pp. 75–78.
3. Almobaied, M.; Al-Nahhal, H.S.; Arrieta, O.; Vilanova, R. Design a robust Proportional-Derivative Gain-Scheduling control for a magnetic levitation system. *Mathematics* **2023**, *11*, 4040. [CrossRef]
4. Week, E.M.; Wahner, U. Linear magnetic bearing and levitation system for machine tools. *CIRP Ann.* **1998**, *47*, 311–314. [CrossRef]

5. He, Z.; Wen, T; Liu, X.; Suo, Y. Loss Estimation and Thermal Analysis of a Magnetic Levitation Reaction Flywheel with PMB and AMB for Satellite Application. *Energies* **2020**, *15*, 1584. [CrossRef]
6. Xu, F.; Lu, X.; Zheng, T.; Xu, X. Motion Control of a Magnetic Levitation Actuator Based on a Wrench Model Considering Yaw Angle. *IEEE Trans. Ind. Electron.* **2020**, *67*, 8545–8554. [CrossRef]
7. Zhang, K.; Xu, F.; Xu, X. Observer-based fast nonlinear MPC for multi-DOF maglev positioning system: Theory and experiment. *Control Eng. Pract.* **2021**, *114*, 104860. [CrossRef]
8. Peng, R.; Zheng, T.; Lu, X.; Xu, X.; Xu, F. Simulation of a synchronous Planar magnetically levitated motion system based on a Real-Time Analytical Force model. *Energies* **2020**, *13*, 6367. [CrossRef]
9. Jansen, J.; Lierop, C.; Lomonova, E.; Vandenput, A. Modeling of Magnetically Levitated Planar Actuators with Moving Magnets. *IEEE Trans. Magn.* **2007**, *43*, 15–25. [CrossRef]
10. Schaeffel, C.; Katzschmann, M.; Mohr, H.; Gloess, R.; Rudolf, C.; Mock, C.; Walenda, C. D planar magnetic levitation system—PIMag 6D. *J. Mech. Eng.* **2016**, *3*, 15-00111. [CrossRef]
11. Kurita, N.; Inomata, R.; Gruber, W.; Okayasu, T. Examination of flex PCB configuration for a winding of a magnetic levitation motor. In Proceedings of the 2020 23rd International Conference on Electrical Machines and Systems (ICEMS), Hamamatsu, Japan, 24–27 November 2020; pp. 1655–1658.
12. lu, X.; Usman, I. 6D direct-drive technology for planar motion stages. *CIRP Ann.* **2012**, *61*, 359–362. [CrossRef]
13. Hsu, A.; Pelrine, R.; De Gouvea Pinto, R.; Howe, A.S.; Schaler, E.W. Design of a Novel Lunar Transportation System (FLOAT) consisting of Diamagnetically-Levitated Robots on a Flexible Film Track. In Proceedings of the 2023 IEEE Aerospace Conference, Big Sky, MT, USA, 4–11 March 2023; pp. 1–20.
14. Zou, M.; Song, M.; Zhou, S.; Xu, X.; Xu, F. Force and Torque Model of Magnetically Levitated System with 2D Halbach Array and Printed Circuit Board Coils. *Sensors* **2023**, *23*, 8735. [CrossRef]
15. Lee, H.; Lee, S.; Won, S.; Lee J. Optimal design of high-precision maglev system using simulation-based DOE and FEM. *IEE Proc.-Electr. Power Appl.* **2006**, *153*, 773–779. [CrossRef]
16. Saaideh, M.A.; Alatawneh, N.; Janaideh, M.A. Multi-objective optimization of a reluctance actuator for precision motion applications. *J. Magn. Magn. Mater.* **2022**, *546*, 168652. [CrossRef]
17. Li, Z; Wu, Q.; Liu, B.; Gong, Z. Optimal Design of Magneto-Force-Thermal Parameters for Electromagnetic Actuators with Halbach Array. *Actuators* **2021**, *10*, 231. [CrossRef]
18. Guo, L.; Zhang, H.; Galea, M.; Li, J.; Gerada, C. Multiobjective Optimization of a Magnetically Levitated Planar Motor with Multilayer Windings. *IEEE Trans. Ind. Electron.* **2016**, *63*, 3522–3532. [CrossRef]
19. Lohrasbi, S.; Hammer, R.; Essl, W.; Reiss, G.; Defregger, S.; Sanz, W. A Comprehensive Review on the Core Thermal Management Improvement Concepts in Power Electronics. *IEEE Access* **2020**, *8*, 166880–166906. [CrossRef]
20. Moore, L.; Shi, L. Emerging challenges and materials for thermal management of electronics. *Mater. Today* **2014**, *17*, 163–174. [CrossRef]
21. Zaman, M.S.; Michalak, A.; Nasr, M.; Da Silva, C.; Mills, J.K.; Amon, C.H.; Trescases, O. Multiphysics Optimization of Thermal Management Designs for Power Electronics Employing Impingement Cooling and Stereolithographic Printing. *IET Power Electron.* **2021**, *36*, 12769–12780. [CrossRef]
22. De Bock, H.P.; Huitink, D.; Shamberger, P.; Lundh, J.S.; Choi, S.; Niedbalski, N.; Boteler, L. A system to package perspective on transient thermal management of electronics. *J. Electron. Packag.* **2020**, *142*, 041111. [CrossRef]
23. Mendizábal, J.K.; Montazeri, M.; Huitink, D.; Miljkovic, N. Direct cooling of a planar magnetic converter using dielectric liquid forced convection enabled by additive manufacturing. *Int. J. Heat Mass Transf.* **2022**, *191*, 122809. [CrossRef]
24. Bancel, F. Magnetic nodes. *J. Phys. D Appl. Phys.* **1999**, *32*, 2155–2161. [CrossRef]
25. Kahaner, D.; Moler, C.; Nash, S. *Numerical Methods in Software and Analysis*; Prentice-Hall: Englewood Cliffs, NJ, USA, 1989.
26. Elleaume, P.; Chubar, O.; Chavanne, J. Computing 3D Magnetic Field from Insertion Devices. In Proceedings of the 1997 Particle Accelerator Conference, Vancouver, BC, Canada, 16 May 1997; pp. 3509–3511.
27. Lu, X.; Zheng, T.; Xu F.; Xu, X. Semi-Analytical Solution of Magnetic Force and Torque for a Novel Magnetically Levitated Actuator in Rotary Table. *IEEE Trans. Magn.* **2019**, *55*, 1–8. [CrossRef]
28. Zhu, H.; Pang, K.; Teo, J. Analysis and control of a 6 DOF maglev positioning system with characteristics of end-effects and eddy current damping. *Mechatronics* **2017**, *47*, 183–194. [CrossRef]
29. Golub, G.; Welsch, H. Calculation of Gauss quadrature rules. *Math. Comput.* **1969**, *23*, 221–230. [CrossRef]
30. Bergman, T.L.; Lavine, A.S.; Incropera, F.P.; Dewitt, D.P. *Fundamentals of Heat and Mass Transfer*, 8th ed.; Wiley: New York, NY, USA, 2017.
31. Akbari, M.; Rezaei-Zare, A. Thermal Analysis of Power Transformers Under Geomagnetically Induced Current. *IEEE T Power Deliver.* **2023**, *38*, 4114–4121. [CrossRef]
32. Ordonez, L.C.; Exposito, A.D.; Cervera, P.A.; Bakic, M.; Wijekoon, T. Fast and Accurate Analytical Thermal Modeling for Planar PCB Magnetic Components. *IEEE Trans. Power Electron.* **2023**, *38*, 7480–7491. [CrossRef]

33. Cengel, Y. *Heat and Mass Transfer: A Practical Approach*, 3rd ed.; McGraw-Hill: New York, NY, USA, 2007 .
34. Zhang, Y. Improved Numerical-Analytical Thermal Modeling Method of the PCB with Considering Radiation Heat Transfer and Calculation of Components Temperature. *IEEE Access* **2021**, *9*, 92925–92940. [CrossRef]
35. Zhang, Y. Modeling Methodology for Reliability-Concerned Current Density Analysis of PCB Tracks and Thermal Analysis of PCB Structure. Ph.D. Dissertation, Department of Information Engineering, University of Pisa, Pisa, Italy, 2013.
36. Yang, C.; Xia, Y. A multi-objective optimization strategy of load-dependent sensor number determination and placement for on orbit modal identification. *Measurement* **2022**, *200*, 111682. [CrossRef]
37. Nourmohammadi, A.; Asteraki, M.H.; Feiz, S.; Habibi, M. A generalized study of coil-core-aspect ratio optimization for noise reduction and snr enhancement in search coil magnetometers at low frequencies. *IEEE Sens. J.* **2015**, *15*, 6454–6459. [CrossRef]
38. Shiri, A.; Allahyari, M. Sensitivity analysis and optimization of railguns using circuit model. *IEEE Trans. Plasma Sci.* **2020**, *48*, C2. [CrossRef]
39. Wang, D.; Tan D.; Liu, L. Particle swarm optimization algorithm: An overview. *Soft Comput.* **2017**, *22*, 387–408. [CrossRef]
40. Goldbarg, E.; Souza, G.; Goldbarg, M. Particle swarm optimization for traveling salesman problem. In Proceedings of the EvoCOP2006, Budapest, Hungary, 10–12 April 2006; pp. 99–110.
41. Parvin, M.; Yousefi, H.; Noorollahi, Y. Techno-economic optimization of a renewable micro grid using multi-objective particle swarm optimization algorithm. *Energy Convers. Manag.* **2023**, *277*, 116639. [CrossRef]
42. Baktash A.; Vahedi, A. Design of a wound core pulse transformer using multiobjective optimization method. *IEEE Trans. Plasma Sci.* **2015**, *43*, 857–863. [CrossRef]